A Risk-Informed Multicriteria Framework for Ocean Current Energy Site Selection for Small Island Developing States

Hafeez O. Oladejo[1,*], Gaël Alory[2], Rasheed B. Adesina[3], Diana N. Bernstein[1], Jonathan Gula[4,5]

[1]*The University of Southern Mississippi, Division of Marine Science, Stennis Space Center, Mississippi, USA.*

[2]*Université de Toulouse, LEGOS (CNES/CNRS/IRD/UT), Toulouse, France*

[3]*Department of Marine Science and Technology, Federal University of Technology, Akure 340252, Nigeria*

[4]*Univ Brest, CNRS, Ifremer, IRD, Laboratoire d'Océanographie Physique et Spatiale (LOPS), IUEM, Plouzané, France.*

[5]*Institut Universitaire de France (IUF), Paris, France.*

Abstract

Small Island Developing States (SIDS) such as Cabo Verde (CV) face persistent energy insecurity due to heavy reliance on imported fossil fuels and limited deployment of land-based renewables. This study develops a transferable, risk-informed multicriteria decision analysis (MCDA) framework for ocean current energy site selection, integrating high-resolution hydrodynamic modeling, environmental constraints, techno-economic factors, and tropical cyclone (TC) exposure. Using a high-resolution ocean circulation model that resolves tidal and inter-island flow dynamics, we characterize the spatial and temporal variability of surface currents and associated power densities across CV. These resource layers are combined with depth, distance-to-coast, protected areas, shipping routes, and TC hazard fields within an MCDA structure supported by sensitivity analysis. Results show that the strongest and most persistent currents occur within the northwestern inter-island channels, where seasonal mean speeds exceed 0.7 m/s and power densities surpass 200 W/m², with 95th-percentile speeds above 2 m/s. Several locations meet key feasibility thresholds with mean currents near or above 1 m/s, suitable depths (10–20 m), proximity to shore, and relatively low variability while also lying outside high-TC-risk zones, low wave conditions, and major maritime corridors. The proposed framework demonstrates how hazard-aware, multi-criteria evaluation can support resilient OCE planning in SIDS and is transferable to other cyclone-exposed coastal systems.

Keywords: Marine Renewable Energy; Ocean Current Energy; Cabo Verde; Multicriteria Decision Analysis; Tropical Cyclone.

Corresponding author: Hafeez O. Oladejo

1.0. Introduction

Achieving a zero-emissions global energy system by 2050 is essential to mitigate the accelerating environmental and climatic impacts of greenhouse gas emissions[1]. Rising energy demand, largely met by fossil fuels continues to drive CO_2-induced warming and increasing the frequency of extreme climatic events[2]. Diversifying renewable energy (RE) portfolios is therefore critical for long-term energy security and climate resilience.

While wind and solar dominate current renewable energy deployment, marine energy (ME) resources remain comparatively underexploited despite their high energy density and predictability[3,4]. Ocean currents, tides, and waves have the potential to complement variable land-based wind and solar resources and contribute quasi-baseload characteristics within diversified RE systems[5]. However, the practical deployment of ocean energy technologies is constrained by engineering complexity, high capital costs, environmental considerations, and operational risks. Consequently, most ME technologies remain at early stages of commercial development. Addressing these challenges requires detailed spatiotemporal resource assessments[6], shoreline evolution and vulnerability[7-9], and improved decision-support methodologies.

These challenges are amplified in Small Island Developing States (SIDS), where geographic isolation, limited domestic resources, and small energy markets drive heavy dependence on imported fossil fuels[10]. This dependence results in high electricity costs, vulnerability to fuel-price volatility, and reduced energy resilience. For many island nations, locally available marine resources represent a strategic opportunity to enhance energy independence while reducing emissions and long-term costs.

Among ME resources, ocean current energy (OCE) is particularly promising due to its inherent predictability, whether driven by the regular astronomical forces, with less minimal susceptibility to weather fluctuations, or by large-scale persistent circulation patterns. OCE is also characterized by relatively high-capacity factor (ratio of the actual energy output of a facility to its maximum possible output over a given period), approximately twice that of wind energy[11]. However, technological, economic, and operational barriers have limited OCE to early-stage deployment, with most projects remaining at pilot or demonstration scales[11,12], highlighting the need for improved resource characterization, optimized site-selection frameworks and deployment methodologies. Further, existing OCE studies have focused primarily on regions with stable

circulation regimes and limited exposure to extreme events, leaving significant methodological gaps in environments where resource variability and hazard exposure are high.

Optimal ME planning has evolved beyond identifying areas of high resource potential. Viable sites must satisfy techno-economic feasibility, environmental constraints, grid accessibility, other maritime uses (e.g., fishing, shipping), and safety considerations, all of which may conflict and complicate decision-making[13,14]. Multicriteria decision analysis (MCDA) has therefore become a widely used tool in RE planning[15]. Among the various MCDA approaches, the analytical hierarchy process (AHP) remains one of the most widely applied due to its simplicity, transparency, and effectiveness in structuring complex decisions[16]. However, despite growing use of MCDA in renewable energy studies, applications to marine-based resources remain limited[16], and criteria sensitivity analyses which are critical for evaluating the robustness of MCDA outcomes are often absent[17,18]. Geographically, only a small fraction of MCDA-based marine energy studies focus on SIDS[16], and none have examined remote island systems such as Cabo Verde. Recent regional energy assessments also reveal methodological gaps, including limited integration of spatiotemporal variability, lack of dynamic environmental hazards[19-22], limiting their ability to support resilient long-term planning.

Cabo Verde (CV), located in the eastern tropical Atlantic between 14°–18°N and approximately 500 km off West Africa, provides a compelling case study. The archipelago comprises ten islands (9 inhabited), several islets (Fig. 1) and remains heavily dependent on imported fossil fuels due to the absence of domestic reserves and relatively low renewable penetration[23]. Electricity prices in CV are among the highest globally and exceed those of major economies (Supplementary Fig. S1). Although the government has set a goal for 100% renewable electricity generation, which was recently revised to 2040 from 2020 due to slow progress[10]. Achieving this requires accelerated research and investment in diverse renewables including ocean energy. Currently, RE (land-based wind and solar) constitutes a small fraction of CV's total energy consumption which has been declining since 1990s (Supplementary Fig. S1). Research has also largely focused on land-based sources[24-26], or wave energy[27-29]. No prior assessment of OCE potential exists for the archipelago, nor has any MCDA-based site-selection framework been developed.

Aside from local energy transition, CV provides a scientifically valuable testbed characterized by features rarely found together in previous OCE studies. First, it has a dynamic oceanographic

setting strongly influenced by the seasonal north–south migration of the Intertropical Convergence Zone (ITCZ), driving pronounced seasonal variability in surface currents as well as mesoscale eddies[30-32]. These necessitate detailed spatiotemporal characterization of local ocean current speeds and power densities. Second, CV has deep-water bathymetry close to shore, and fragmented island grids with limited interconnection (Fig. 1). Third, the archipelago also lies within the Main Development Region for tropical cyclones (TC). This combination creates a complex decision landscape that challenges existing OCE assessment and MCDA methodologies, making CV not only a relevant case study but also an ideal environment for methodological advancement. Despite impacts of TCs on offshore structures including intensified currents, enhanced shear and turbulence[33], increased structural loads and fatigue[34], heightened mooring and cable failure risks[35], no existing MCDA frameworks for marine energy explicitly incorporate cyclone hazard. Integrating TC risk marks a conceptual shift toward risk-informed MCDA.

This study addresses these research gaps by providing the first comprehensive assessment of OCE potential in CV. Using high-resolution ocean current data, we characterize the spatial and temporal variability of OCE across the archipelago and evaluate its technical feasibility. We further develop and apply an MCDA framework to identify optimal extraction sites by simultaneously considering resource magnitude, variability, techno-economic factors, environmental constraints, grid proximity, and tropical cyclone exposure. By explicitly integrating TC risk into the decision framework, this study introduces a risk-informed methodology for marine energy planning in SIDS, providing a transferable approach to other cyclone-exposed islands or coastal areas for resilient and sustainable ocean energy development.

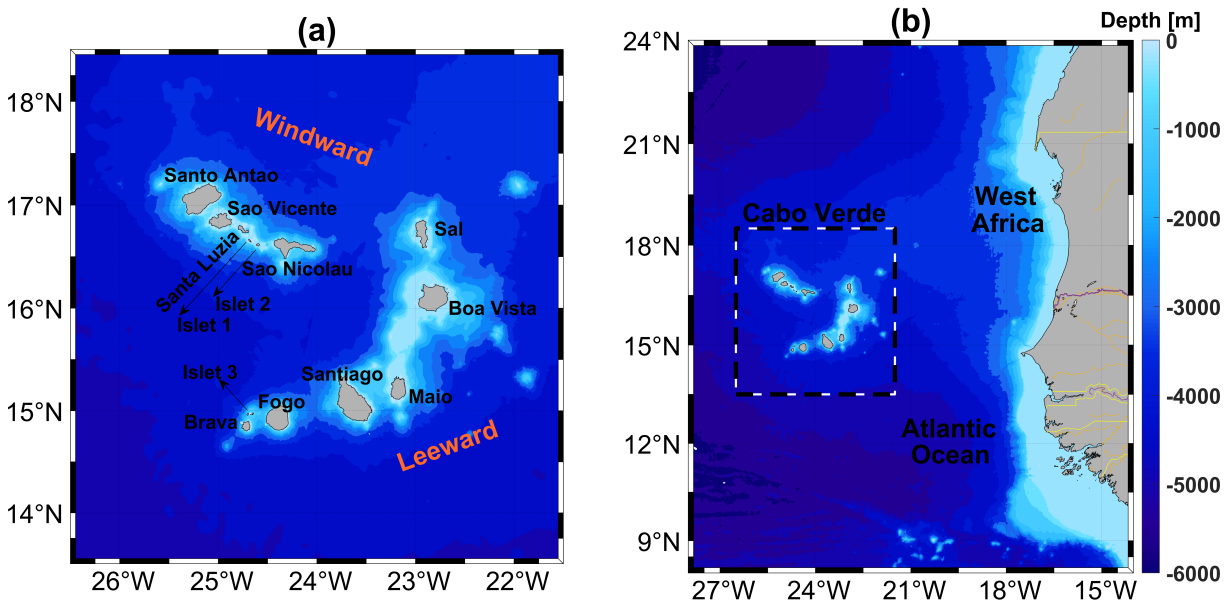

115

116 ***Fig.1. Bathymetry maps of the study area (a) CV, (b) Larger-scale section of the Atlantic Ocean***
117 ***off West Africa. The Southern islands of CV are Brava, Fogo, Santiago, and Maio, with Boa***
118 ***Vista and Sal to make Leeward islands while the Windward islands are Santo Antão, São***
119 ***Vicente, Santa Luzia (uninhabited), and São Nicolau.***

120 **2. Methods**

121 This study focuses on ocean current energy, which is a major form of energy from the ocean aside
122 from waves, offshore winds, and salinity gradients. We utilized high-resolution numerical
123 simulation outputs to evaluate OCE potential with its spatial and temporal variability. In addition,
124 datasets on electricity prices, renewable energy consumption, bathymetry, coastal proximity,
125 marine protected areas, ship ports, and TC were obtained and processed as input for an MCDA
126 model to evaluate the energy state and identify energy hotspots and optimal energy extraction sites.
127 All data sources are listed in Supplementary Table S1.

128 **2.1. Ocean Current Datasets**

129 This study uses surface ocean current data extracted from a submesoscale-permitting Atlantic wide
130 simulation[36](GIGATL1). It is performed with the Coastal and Regional Ocean Community
131 Model[37], which is built upon the Regional Ocean Modeling System[38]. We use one year of data

from June 2008 to May 2009 in this study (Supplementary Table S1). GIGATL1 has an hourly temporal resolution, a horizontal resolution of 750 m, and 100 topography-following vertical levels. GIGATL1 is initialized from a lower resolution version (3 km) of an otherwise identical configuration initialized in January 2004, with boundary conditions supplied by the Simple Ocean Data Assimilation model. For this study, we use the simulation that includes tidal forcing to account for the total ocean current in the study area. Further details on the model can be found at https://github.com/Mesharou/GIGATL/.

To evaluate the performance of GIGATL1, we extracted ocean current information from quality-controlled drifter data (Index of /data/oceans/aoml/gdp), and collocated the model and observational data in both time and space following Oladejo et al.[39]. The model agrees well with observations, with a bias of 3% and a root-mean-square error (RMSE) of 0.12 m s^{-1} (Supplementary Fig. S2). Quantitative evaluation was also conducted against several global ocean current datasets, including the Copernicus Marine Environment Monitoring Service (CMEMS) global analysis and forecast product (50 vertical layers, 8 km horizontal resolution, 6-hour temporal resolution), the Hybrid Coordinate Ocean Model (HyCOM) dataset (50 vertical layers, 8 km horizontal resolution, 3-hour temporal resolution), and the Ocean Surface Current Analyses Real-time (OSCAR) dataset (30 m surface average, 25 km horizontal resolution, daily temporal resolution) (see Supplementary Table S1 for data sources and Supplementary Fig. S3 for data comparison).

The comparison revealed that these datasets failed to adequately resolve the CV Island system, showing substantial data gaps in the surrounding waters (Supplementary Fig. S3). While they captured some strong currents in the southwestern and western regions of CV, they did not resolve the strongest currents (i.e., those current flowing between the islands). In contrast, GIGATL1, with its finer horizontal and vertical resolutions and inclusion of tides, better captured the islands and their surrounding currents, including inter-island and islet currents, making it the most appropriate dataset for this study (Appendix B).

2.2 Ocean Current Energy and Variability

Ocean current energy can be harnessed using underwater turbines that convert the mechanical energy of the ocean currents into electricity. There has been significant research progress in energy converters that can enhance even the least obtainable current energy. The available in-stream power per unit area, or power density (W/m^2), is calculated using Eq. 1 below:

$$P = \frac{1}{2} \cdot \rho \cdot P_l^{\,3} \qquad (1)$$

Where P is the ocean power or current density (OCD), ρ is the density of water, and P_l represents the power available at the individual device level is given by Eq. 2 as:

$$P_l = \sqrt{u^2 + v^2} \qquad (2)$$

where P_l is the magnitude of the velocity derived from the meridional (v) and zonal (u) current velocities.

Assuming some electrical or mechanical energy losses during operation, the theoretical power Tp (Watts) generated by a turbine can be computed as Eq.3:

$$Tp = A \cdot \eta \cdot P \qquad (3)$$

Where A is the swept area of the turbine rotor ($=\pi D^2/4$; where D is the rotor diameter), η is the turbine efficiency. Prototype-scale tidal stream and ocean current turbines commonly achieve power coefficients in the range of 0.30–0.45; therefore, we adopt the upper end of this range of 45% as a representative practical value which is consistent with the Betz limit (maximum theoretical efficiency) of 59.3%[40]. A rotor diameter of 20 m was assumed consistent with values reported for contemporary prototype-scale OCE devices. To account for spatial deployment potential, an array density of X turbines km^{-2} was applied, corresponding to inter-turbine spacings of approximately Y rotor diameters along-stream and Z rotor diameters cross-stream, consistent with typical marine hydrokinetic array design practice. We assume X = 30 turbines per square kilometer.

Additional statistical analyses, such as the coefficient of variation (CoV) and monthly variability index (MVI), were used in this study for evaluating site variation over time and for identifying the hotspot zone. The CoV is a statistical parameter that determines site variability by dividing the standard deviation of daily averaged current data at each station by the overall mean across the study period at that station. The MVI, previously applied in wave energy[41], is the ratio of the monthly energy range (i.e., the monthly highest minus lowest) with the mean. A high MVI and CoV indicate greater variability, whereas low values suggest a more stable energy resource.

2.3. Optimal Energy and Hotspot Zones with AHP

2.3.1. Other Datasets for AHP Analysis

The optimal location for OCE in CV was determined using bathymetry, distance from the coast, and historical TC datasets as key geospatial criteria.

The bathymetry dataset was sourced from NOAA's latest "Earth TOPOgraphy" dataset, ETOPO22, designed for coastal hazard and tsunami modeling[42]. ETOPO22 is a continuous global gridded terrain model covering both ocean and land with a spatial resolution of 15 arc-seconds (~450 m). The dataset integrates multiple sources, including airborne lidar, satellite-derived topography, and shipborne bathymetry, combining data from major repositories including General Bathymetric Chart of the Oceans 2022, Global Multi-Resolution Topography (v4.0), Copernicus DEM 30m, Continuously Updated Digital Elevation Models. Additionally, ETOPO22 incorporates bare-earth topographic data from NASA's ICESat-2 and other data sources to independently validate both the input datasets and the final model[43].

The distance from the coast dataset was derived from NASA's global coastal distance dataset at 0.1-degree resolution (https://oceancolor.gsfc.nasa.gov/resources/docs/distfromcoast/). This dataset provides accurate measurements of coastal proximity, which is crucial for evaluating accessibility and feasibility for OCE deployment.

The historical TC dataset (1851-2024) for the CV region was obtained from the International Best Track Archive for Climate Stewardship (IBTrACS)[44]. We applied a Kernel Density Estimation (KDE) function weighted by storm intensity to estimate the spatial likelihood of TC passage and account for the impact of storm intensity. For KDE functions and their applications, see Soh et al.[45] and Węglarczyk[46]. Here, we employed a gaussian kernel with a bandwidth of 0.5°, which corresponds approximately to a spatial influence radius of 50–60 km. The integrated storm frequency and intensity give a single hazard metric fed into the MCDA model. The KDE function is given by Eq. 4:

$$f(x) = \frac{1}{nh}\sum_{i=1}^{n} K\left(\frac{x - x_i}{h}\right) \qquad (4)$$

where the gaussian kernel function (K) can be expressed by Eq. 5:

$$K(u) = \frac{1}{\sqrt{2\pi}} e^{-\frac{1}{2}u^2} \qquad (5)$$

Hence, n is the total number of track points, h is the bandwidth (0.5°), x_i are the coordinates of each storm data point, x are the coordinates of the final grid. In our case, the estimated TC-hazard exposure is expressed by Eqs. 6 and 7, where the planar distance term $x - x_i$ is replaced by d_i, which is the great-circle distance between the grid point x and the i-th storm track point, computed using the Haversine formula:

$$f(x) = \sum_{i=1}^{n} w_i \cdot exp\left(-\frac{{d_i}^2}{2h^2}\right) \qquad (6)$$

$$d_i = 2R \cdot \arcsin\left(\sqrt{\sin^2\left(\frac{\Delta\phi_i}{2}\right) + \cos(\phi_1)\cos(\phi_2)\sin^2\left(\frac{\Delta\lambda_i}{2}\right)}\right) \qquad (7)$$

where w_i is the normalized wind speed of the i-th storm point, with weights scaled so that their sum equals one to ensure proper KDE normalization, $R = 6371$ km (Earth's radius), $\phi_1 \; and \; \phi_2$ are latitudes (in radians) of the grid point and the i-th storm point, respectively, and $\Delta\phi_i$ and $\Delta\lambda_i$ are the differences in latitude and longitude between them.

Lastly, we examined six years of satellite significant wave height (swh) and wind speed data (2020–2025) to identify areas exposed to high wave energy (Supplementary Table S1 for data source). The data were extracted from seven multi-mission altimetry satellites including Sentinel-3A, Sentinel-3B, Sentinel-6A, Jason-3, CryoSat-2, SARAL, and SWOT, yielding 1,114,895 data points over this period. The extracted variables provide a practical first-order proxy for coastal forcing, which can be linked to erosion potential, wave setup, and nearshore hydrodynamic stress. This screening allows us to distinguish energetic zones, where cable landfalls and nearshore infrastructure may face elevated morphodynamical risk, from more sheltered areas that offer greater stability for installations. In addition to wind-driven hazards, tropical cyclones often generate storm surges, wave setup, and elevated bottom shear stress, all of which can significantly alter nearshore hydrodynamics and infrastructure exposure[39,47](Supplementary Fig. S4). These

coupled effects further justify the strong hazard penalties applied to TC-prone regions, highlighting the need to also avoid hyper energetic coastal segments in the final suitability zonation.

2.3.2. AHP Procedure

The AHP is a widely used multi-criteria decision-making model that derives priority scales from pairwise comparisons. In this study, AHP is applied to identify optimal zones for OCE extraction by ranking key criteria and sub-criteria based on their relative importance.

According to Saaty[48], solving a multi-criteria problem requires analyzing its characteristics and structuring it into well-defined components. Hence, AHP ranks the problem into main criteria and sub-criteria, and generates their weight based on their pairwise relationships. In this context, we categorize the problem into three main criteria: energy resources, environmental constraints, and techno-economic considerations.

Site Selection Considerations

Several factors influence the feasibility of marine energy extraction, particularly water depth and distance from shore[49]. Typically, energy resources should be within 25 km of the coastline to minimize both transmission costs and energy losses over long distances, while 2-5 km buffer zones may be necessary to avoid conflicts with shipping routes. Additionally, water depth dictates the choice of turbine support structures (e.g., seabed vs moored or floating platforms).

Furthermore, the potential OCE sites we are evaluating within the study area all fall well within CV's Exclusive Economic Zone (EEZ), which extends up to 200 nautical miles from the coastline. This ensures that all selected locations remain under national jurisdiction, with no legal constraints on marine resource utilization.

Another critical factor is marine biodiversity and conservation areas. CV hosts numerous endemic marine species, and several Protected Areas (PAs) of about 50 exist across the region. As illustrated in Fig. 2, these PAs are categorized into marine-exclusive, terrestrial-exclusive, and mixed zones. Additionally, fishing and tourism contribute significantly to CV's economy, though comprehensive datasets on these activities remain limited. The source of both EEZ and PAs datasets are provided in Supplementary Table 1. PAs are sourced from the World Database on PAs.

Further, areas with a high risk of exposure to TC should be avoided.

Thus, the sub-criteria for AHP model include:

i. Energy resources: Ocean power/current density (OCD) and variability
ii. Environmental constraints: accounting for overlaps with Marine, terrestrial, and mixed PAs (Fig 2)
iii. Techno-economic factors: Depth, distance to the coast (D2C), and the effects of TCs (Fig. 2 and Supplementary Fig. S5).

AHP Weighting and Sensitivity Analysis

The AHP methodology, along with its mathematical formulation, is detailed in S3. The pairwise comparison matrix and weight assignments were derived from synthesis of previous studies[14-18], with regional energy priorities modification (Table 1). This structured synthesis of weighting logic reported in recent offshore renewable energy siting studies were based on expert opinions, surveys, and extensive literature reviews. These studies collectively emphasize the relative importance of energy resources, environmental sensitivity, and techno economic feasibility, with variations depending on regional context. We adapted these established priority structures to the Cabo Verde setting using domain knowledge of local energy planning needs, land and marine use, and economic reliance. For example, Salvador et al. emphasized environmental and seabed constraints such as marine reserves, restricted areas, and seabed topography as essential criteria, while Majidi et al. found that experts consistently ranked the energy resource and operational availability above seabed characteristics. Solbrekke & Sorteberg prioritized energy resource quality and techno-economic factors (depth, distance to infrastructure), with environmental sensitivity occasionally receiving higher weight than met-ocean constraints. Johnston et al. similarly highlighted resource strength, depth, distance to shore, and conservation areas as key determinants of deployment feasibility.

As with other MCDA approaches (including fuzzy AHP and Bayesian extensions), some degree of subjectivity is inherent in the weighting process. Consideration of these different perspectives in site prioritization led to the establishment a scenario-based sensitivity assessment through four weighting configurations to represent systematic variations in the relative importance of the criteria and account for uncertainty in weighting options:

1. C1: Equal importance assigned to all criteria.

2. C2: Higher priority to energy resources, followed by techno-economic factors, with environmental constraints given the least priority. Within sub-criteria: ocean power density prioritized over its variability.
    i. Marine PAs is given higher importance than mixed, which in turn outweighs terrestrial PAs, reflecting stricter ecological protection, the presence of endemic marine species, and Cabo Verde's reliance on fisheries.
    ii. Depth ranked higher than D2C, considering that CV's seafloor deepens more rapidly in most areas than the horizontal increase in D2C (Figs. 1 and 2). Bathymetry also varies at a non-constant rate (Supplementary Fig. S5) and is a key factor in determining the appropriate support structure for OCE deployment.
3. C3: Energy is given even greater priority (10% higher than in C2), which slightly reduces the weights of other pairwise comparisons of C2 (Table 1).
4. C4: Same as C3 but with the influence of the effects of TC.

The output of the AHP model is a final suitability score, which was used to classify CV's coastal waters into highly suitable, suitable, moderately suitable, and non-suitable zones. Additionally, areas beyond 1000 m depth and more than 10 km offshore are designated as excluded zones, automatically categorized as non-suitable due to feasibility constraints.

Table 1 summarizes the criteria, sub-criteria, and final weight assignments based on the AHP. The relative priority scale used to derive the weights, along with the Consistency Ratio (CR), is provided in Supplementary Section S3. Note: Supplementary Tables S2 and S3 present Saaty's scale of importance and the corresponding consistency index, while Supplementary Table S4 shows the pairwise comparison for the main and sub-criteria across the four scenarios in this study, and Supplementary Table S5 reports the resulting CR values.

Criteria	W (C1)	W (C2)	W (C3)	W (C4)	sub-Criteria	s-W (C1)	s-W (C2)	s-W (C3)	s-W (C4)	g-W (C1)	g-W (C2)	g-W (C3)	g-W (C4)
Energy	0.34	0.46	0.56	0.56	power	0.5	0.875	0.88	0.88	0.17	0.40	0.49	0.49
					variability	0.5	0.125	0.13	0.13	0.17	0.06	0.07	0.07
Environment	0.33	0.22	0.15	0.15	terrestrial	0.33	0.14	0.14	0.14	0.11	0.03	0.02	0.02
					marine	0.34	0.57	0.57	0.57	0.11	0.13	0.09	0.09
					mixed	0.33	0.29	0.29	0.29	0.11	0.06	0.04	0.04

Techno-economical	0.33	0.32	0.29	0.29	Depth	0.5	0.75	0.75	0.6	0.17	0.24	0.22	0.17
					D2C	0.5	0.25	0.25	0.2	0.17	0.08	0.07	0.06
					TC	-	-	-	0.2	-	-	-	0.06
sum	1.00	1.00	1.00	1.00	sum					1.00	1.00	1.00	1.00

321 W=weights; s-W=sub-criteria weights; g-W=global weights

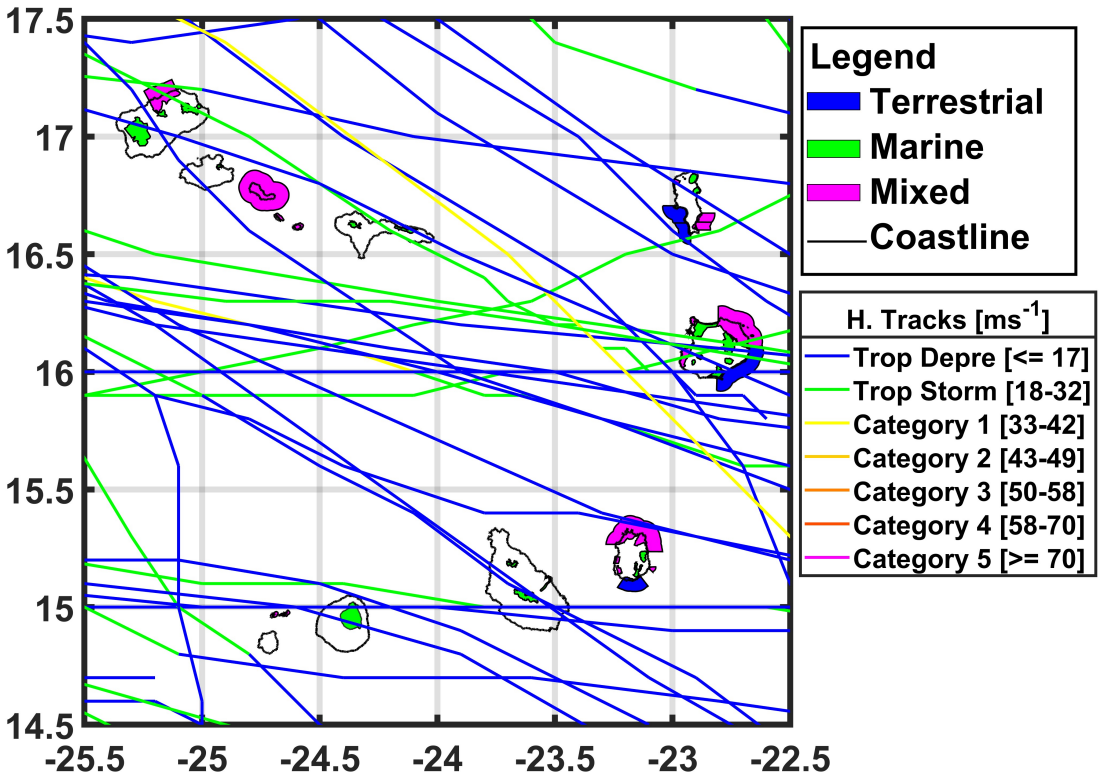

322

323 ***Fig. 2. Protected Areas, and historical TC tracks (1851-2024) for CV (see Appendix A for data***
324 ***source). A total of 2,300 storms originated in or passed through the study area, with 87 storms***
325 ***having at least one data point within the region.***

326 **3. Results**

327 **3.1. Monthly and Seasonal Variability in Ocean Current and OCD across CV**

328 The seasonal and monthly mean distribution of ocean surface current, as illustrated in Fig. 3 and
329 Supplementary Fig. S6, reveals that the strongest currents are predominantly located between the
330 northwestern islands. Notably, the areas between São Vicente and Santa Luzia, as well as Santa

Luzia and the first islet near São Nicolau (Islet 1 in Fig. 1), exhibit consistently high current velocities exceeding 0.9 m/s throughout the year. Some of these currents occasionally extend toward the northwest of Santo Antão. Moderately strong currents, averaging around 0.5 m/s, are observed between Boa Vista and Maio, with their intensity varying seasonally. Overall, currents with velocities around 0.4 m/s are commonly found near the coastlines of many islands, particularly near their tips. In contrast, the weakest currents (< 0.2 m/s) exhibit a spatially variable distribution and are primarily concentrated in the central region of CV far from the coast. The southern islands (Brava, Fogo, and Santiago; excluding Maio), which exhibits strong currents only in its northern region, experience strong seasonal variations in both the intensity and patterns of ocean currents, making them distinct from other areas within the archipelago.

Similarly, the seasonal and monthly mean distribution of OCD, presented in Fig. 3 and Supplementary Fig. S7, indicates that the highest densities are concentrated in the northwestern islands of the archipelago, consistently exceeding 200 W/m² between São Vicente and Santa Luzia, as well as between Santa Luzia and Islet 1 near São Nicolau (Islet 1 in Fig. 1), throughout the year. Moderately high OCD values (80–100 W/m²) are observed in July through September, and JJA in the southwestern region of the archipelago, (a feature not distinctly reflected in the currents in Fig. 3 and Supplementary Fig. S6), as well as around Sal, northern Maio, and between Boa Vista and Maio year-round. These moderately high OCD values extend to other parts of the archipelago, displaying variability in their spatial and temporal distribution over the course of the year.

The monthly mean ocean current and ocean current density averaged over the entire study area is presented in Table 2. The differences in the month-to-month mean current averaged across the area are relatively small, generally ≤ 0.07 m/s, with even smaller differences in the monthly percentiles. However, the month-to-month differences in the mean current densities averaged across the area can reach up to 9 W/m², with percentile differences exceeding 25 W/m². The months of November and December show the lowest values for both the mean and percentiles of current and current densities across the area. In contrast, July, August, and September exhibit the highest mean and percentile values for current densities as shown in Table 2.

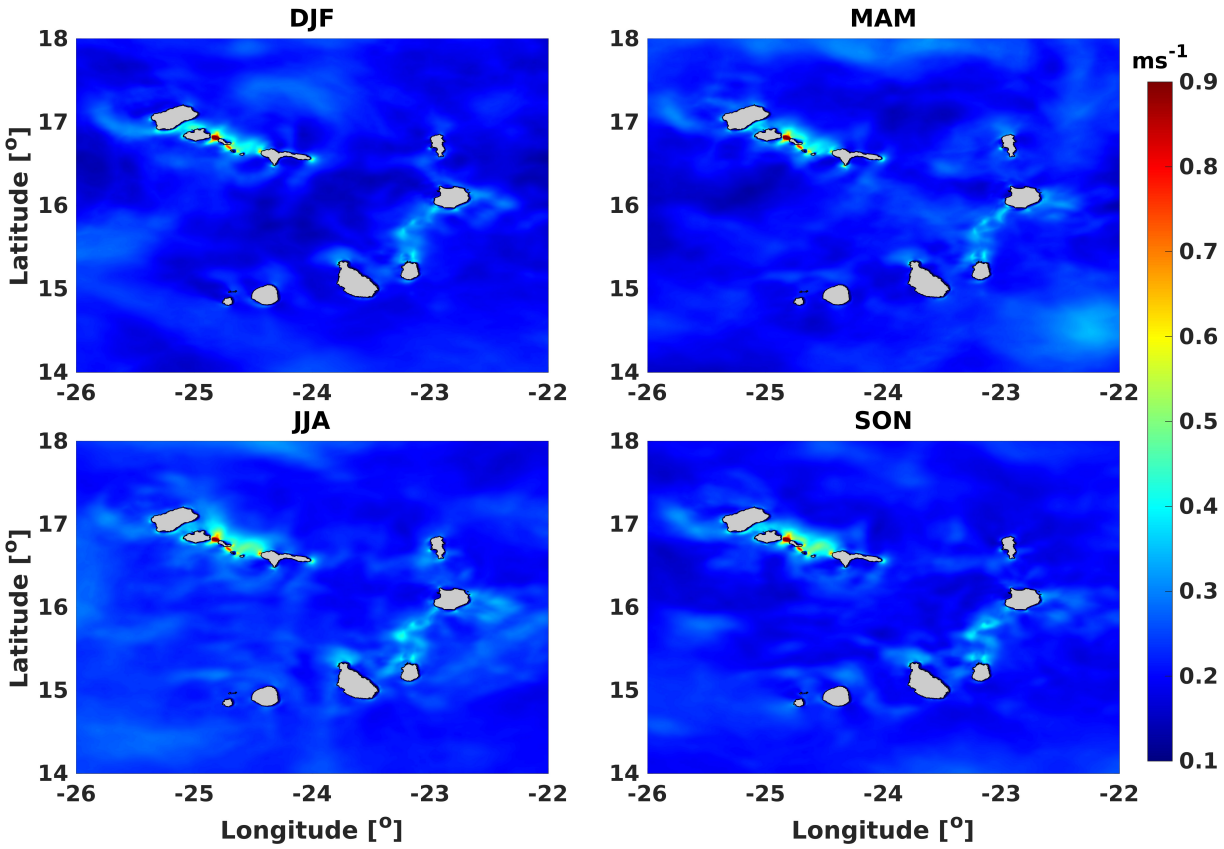

358

359 ***Fig. 3. Seasonal mean ocean current speed [m/s] across the study area. DJF: December–***

360 ***January–February, MAM: March–April–May, JJA: June–July–August, SON: September–***

361 ***October–November.***

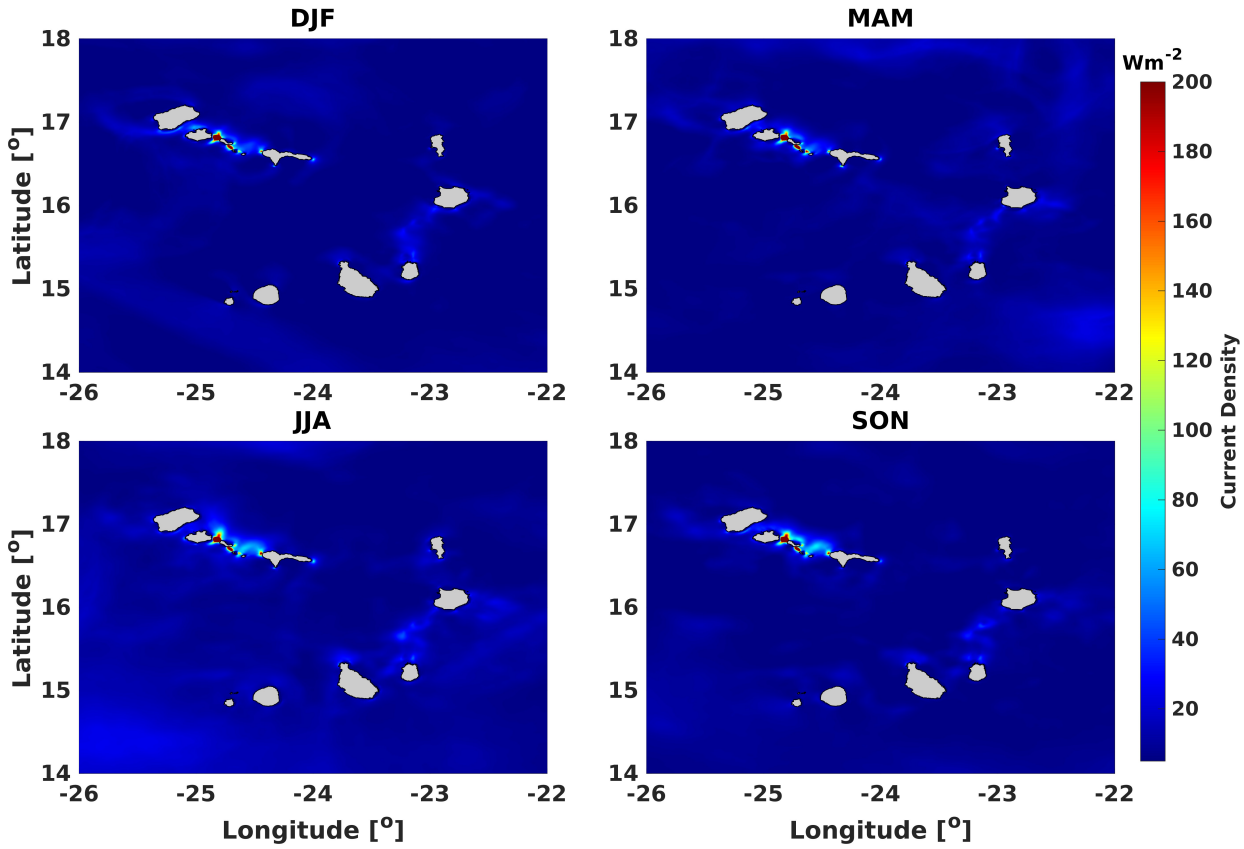

362

363 ***Fig. 4. Seasonal mean current densities across the study area. DJF: December–January–***
364 ***February, MAM: March–April–May, JJA: June–July–August, SON: September–October–***
365 ***November.***

366 ***Table 2. Monthly statistics of ocean current speed (m/s) and density (W/m^2) averaged over the***
367 ***study area***

	ocean current speed					ocean current density				
	mean	P50	P75	P95	P99	mean	P50	P75	P95	P99
Jan	0.21	0.20	0.23	0.29	0.33	6.94	5.22	8.16	15.99	24.22
Feb	0.20	0.19	0.23	0.29	0.35	6.61	4.42	7.77	16.69	30.58
Mar	0.21	0.20	0.24	0.32	0.41	8.56	5.89	10.36	23.94	46.49
Apr	0.22	0.21	0.26	0.33	0.39	10.92	8.67	13.59	27.35	40.12
May	0.21	0.20	0.24	0.31	0.37	7.41	4.88	9.04	19.58	31.73
Jun	0.20	0.19	0.23	0.30	0.39	6.77	4.63	7.33	17.48	35.84
Jul	0.25	0.25	0.28	0.33	0.40	14.18	10.35	18.76	33.14	49.41

Aug	0.24	0.23	0.26	0.31	0.36	10.24	8.82	11.94	20.31	29.33
Sep	0.23	0.23	0.25	0.31	0.36	10.04	8.13	11.94	20.45	30.37
Oct	0.21	0.21	0.24	0.29	0.35	7.41	6.01	8.80	15.91	25.57
Nov	0.18	0.17	0.21	0.28	0.33	5.14	3.23	5.93	13.28	21.48
Dec	0.19	0.18	0.21	0.27	0.33	5.29	3.68	5.77	12.76	23.56

3.2. Statistical Analysis and Variability of OCD

The annual mean OCD across the CV archipelago ranges from less than 10 W/m² to above 200 W/m² (Fig. 5a). The highest mean densities (>200 W/m²) are concentrated around the northern island chains, particularly along the southeastern coast of São Vicente and the eastern and western coasts of Santa Luzia. Current densities approaching 100 W/m² are also observed along the southeastern coast of Santo Antão and the western coast of São Nicolau. Additionally, annual mean current densities exceeding 50 W/m² are present within approximately 10 km of the coastlines of most islands.

The 50th percentile (P50) current density (Fig. 5b) shows a similar spatial distribution pattern to the mean but with reduced values, generally ranging below 10 W/m². However, the highest-density regions such as the coasts of São Vicente and Santa Luzia still exceed 200 W/m². At the 75th percentile, P75 (Fig. 5c) and 95th percentile, P95 (Fig. 5d), current densities rise significantly around the islands, with values surpassing 80 W/m² and 150 W/m², respectively. These increases are particularly notable in the northwestern islands, south of Boa Vista, and north of Maio and Santiago. The northern coasts of Fogo and Brava also show increased densities, reaching approximately 60 W/m² and 80 W/m² at the 75th and 95th percentiles, respectively. In contrast, the central regions of the archipelago exhibit low current densities across all percentiles.

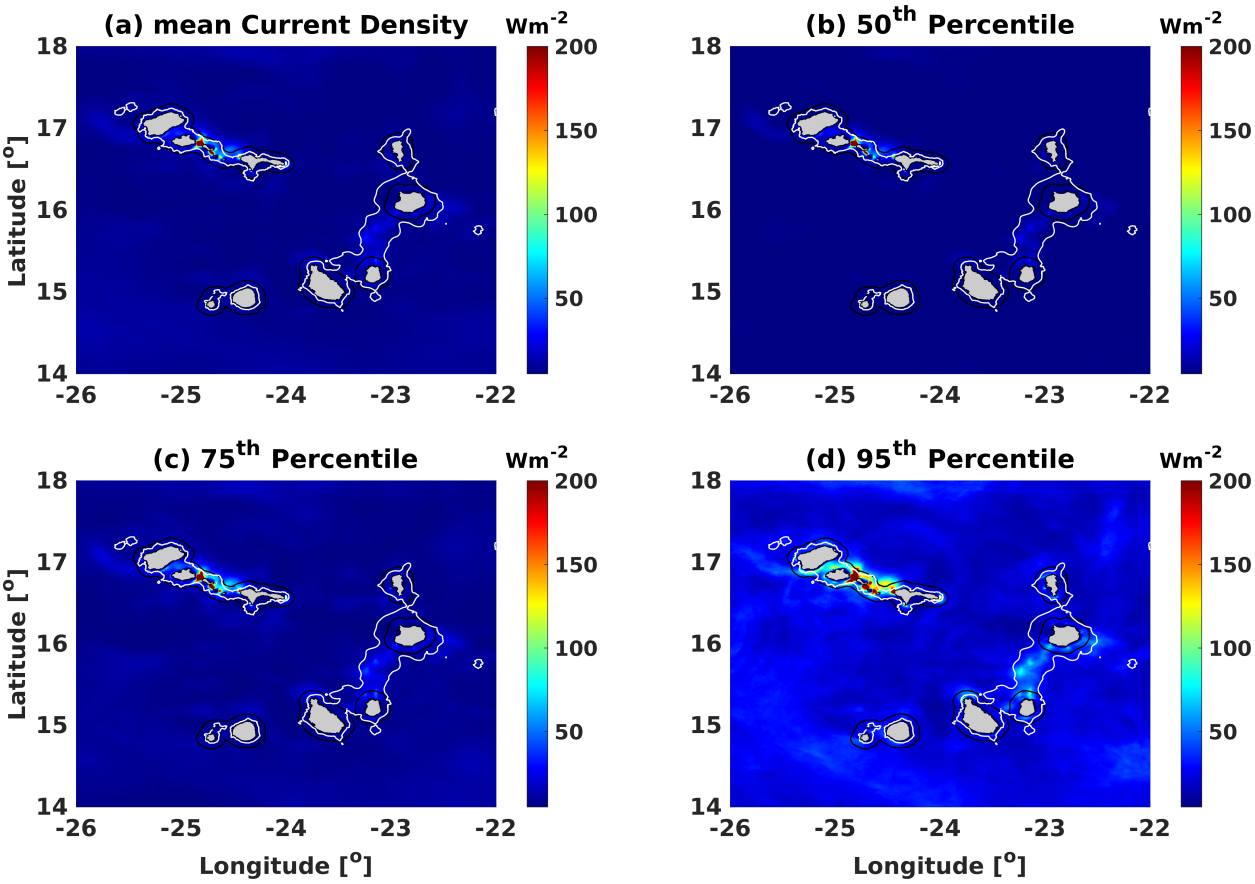

Fig. 5. Spatial variation of annual mean and percentiles of OCDs [W/m2] across the study area. Black and white lines represent 10 km distance from the coast and 1000 m depth respectively while grey are the islands.

The results of the coefficient of variation and monthly variability index are used to assess the site-specific variations in ocean current densities across the Cabo Verde archipelago, as shown in Fig. 8. Similar to the distribution of ocean current and OCDs around the archipelago (Figs. 3 and 4), the site variabilities of OCD (as expressed in CoV and MVI) show that they are highest within some specific areas of the archipelago, mostly areas with lowest current velocities and densities. The CoV (Fig. 6a) has its highest values around the south and southwestern CV as seen in Fig. 1. Additionally, the eastern coasts of Boa Vista, far northern region of Sal, and the western part of the archipelago are regions with relatively high CoV. For MVI (Fig. 6b), elevated values are observed in the eastern and western regions of CV, as well as the southern and southwestern areas. This suggests some distinction between the spatial distributions of CoV and MVI. Interestingly, regions with high CoV and MVI are located outside the 10 km delineated coastal waters of the

northern islands, which correspond to areas with the strongest currents and highest current densities. These areas exhibit low variability in current densities. The southern islands, Fogo, Brava, and Santiago, demonstrate some of the highest CoV and MVI values within their coastal waters, highlighting significant variability in these regions.

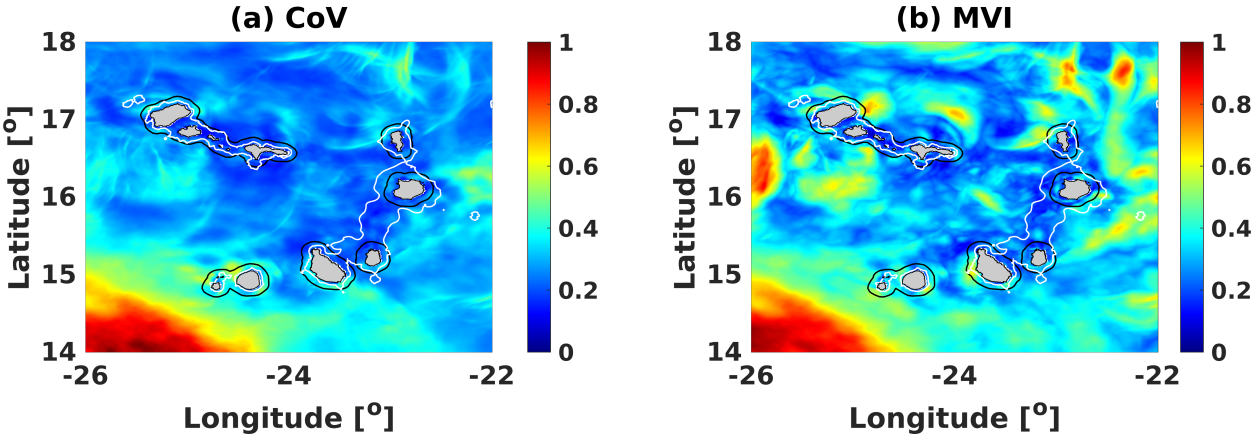

Fig. 6. Spatial variation of CoV and MVI of ocean current densities across the study area. Black and white lines represent 10 km distance from the coast and 1000 m depth respectively while grey are the islands.

3.3. AHP Results

The AHP results (Fig. 7a-d) reveal how different weighting conditions influence the zonation of CV's coastal waters for OCE suitability. In the first condition (C1), where equal priorities are assigned to all criteria and sub-criteria, the resulting zonation is predominantly composed of highly suitable (red), suitable (white), and non-suitable (grey) areas. Highly suitable zones cover most areas within 10 km offshore and depths shallower than 1000 m, while suitable zones appear where environmental factors, PAs, play a dominant role. The remaining areas fall into non-suitable or excluded zones. For example, the wide channel between Boa Vista and Maio, despite having relatively shallow depths and strong current densities, is categorized as non-suitable partly because it extends beyond the 10 km offshore limit. Similarly, in the southern CV region around Fogo and Brava, depths of 1000 m are reached within approximately 2 km of the coast, reducing their suitability score as they may fall within shipping routes and other land usages.

In the second condition (C2), where greater importance is assigned to energy potential over environmental and techno-economic factors, and where depth is weighted more heavily than shoreline distance, most areas remain categorized as non-suitable or excluded zones, similar to C1. However, most of the highly suitable zones in the first scenario is downgraded to the suitable zone. The highly suitable zones in this case are concentrated in the narrow strait between Santo Antão and São Vicente, where the strongest currents and current densities are observed, along with low variability, relatively shallow depths, and proximity to the shore.

The third condition (C3) further refines the classification, reinforcing the exclusion of areas beyond 10 km offshore and 1000 m depth as non-suitable or excluded zones. Most areas within 10 km and 1000 m depth fall into the moderately suitable category. The suitable zones are distributed across the channels between the northwestern island chain, eastern Sal, western and northern Boa Vista, northern and western Maio, and select locations around Santiago, Fogo, and Brava. The highly suitable zones remain concentrated in the same region as in C2, particularly between Santo Antão and São Vicente.

The fourth condition (C4) introduces TC exposure risk as a new constraint within the multicriteria model. This alters the suitability zonation across the study area. While portions of the northwestern island group still retain high suitability, many regions across the eastern and southern islands, including Sal, Boa Vista, Maio, Santiago, Fogo, and Brava, are now downgraded to moderately suitable or not suitable. In these areas, the suitable zones are restricted to isolated coastal tips and narrow nearshore bands, many of which are too limited in size to be visually discerned at the current map scale.

We selected 11 points with the highest mean current speed and current densities around the islands, all of which fall within the highly suitable and suitable zones in Fig. 7c, as potential energy hotspot sites for final site characterization. It is important to note that each selected site likely represents an area with similar energy characteristics within a certain mile radius, as evidenced by the patterns observed in Figs 3–5. In particular, the channel between São Vicente and the uninhabited island of Santa Luzia, which exhibits the strongest currents and highest current density, spans several miles.

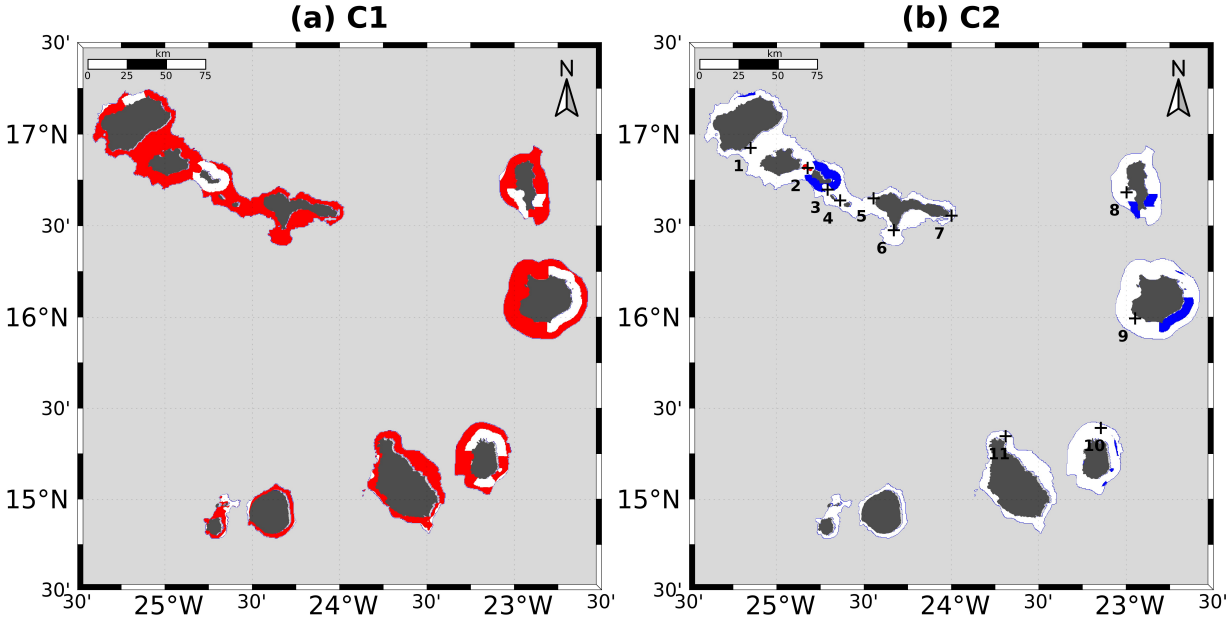
(a) C1
(b) C2
km
0 25 50 75
N
17°N
16°N
15°N
30'
25°W
24°W
23°W
1
2
3
4
5
6
7
8
9
10
11

447

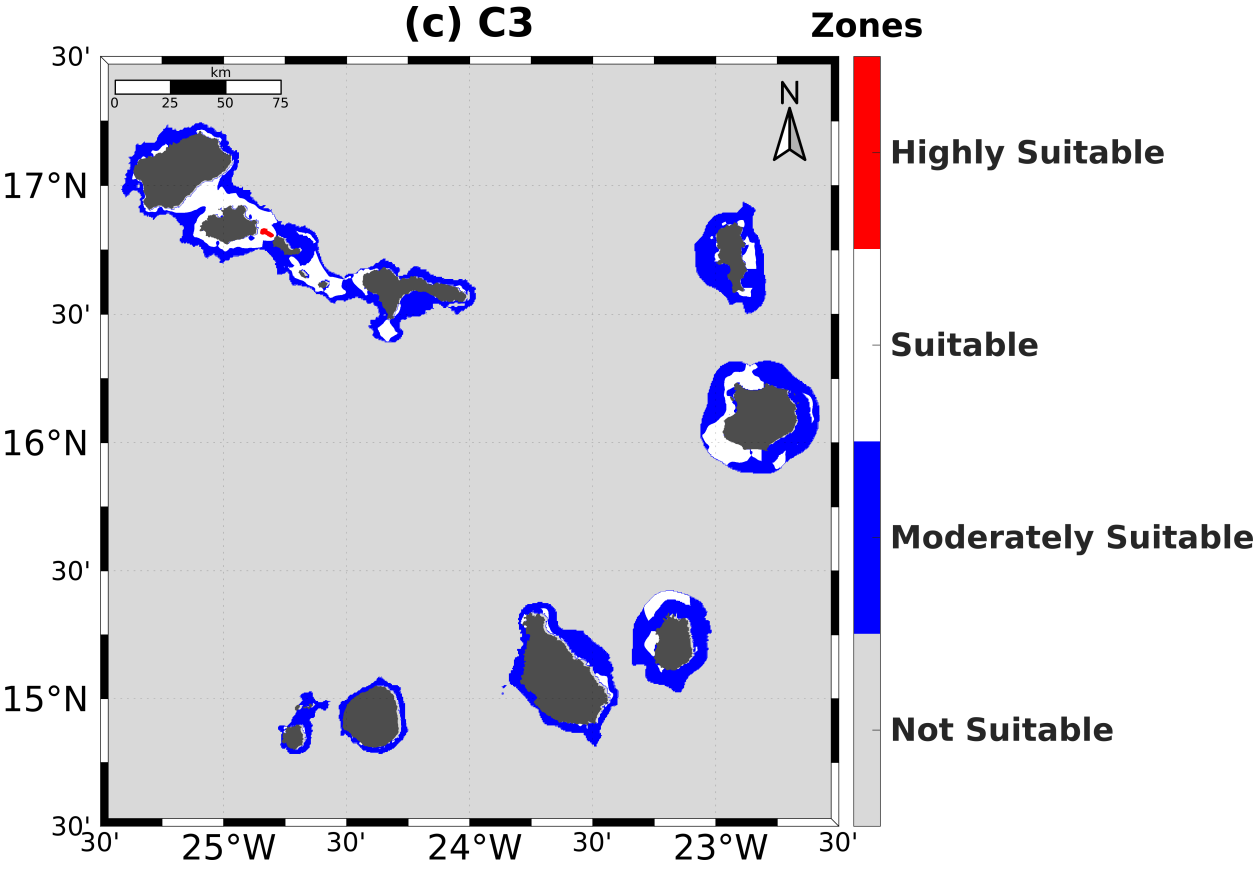
(c) C3
Zones
km
0 25 50 75
N
17°N
16°N
15°N
30'
25°W
24°W
23°W
Highly Suitable
Suitable
Moderately Suitable
Not Suitable

448

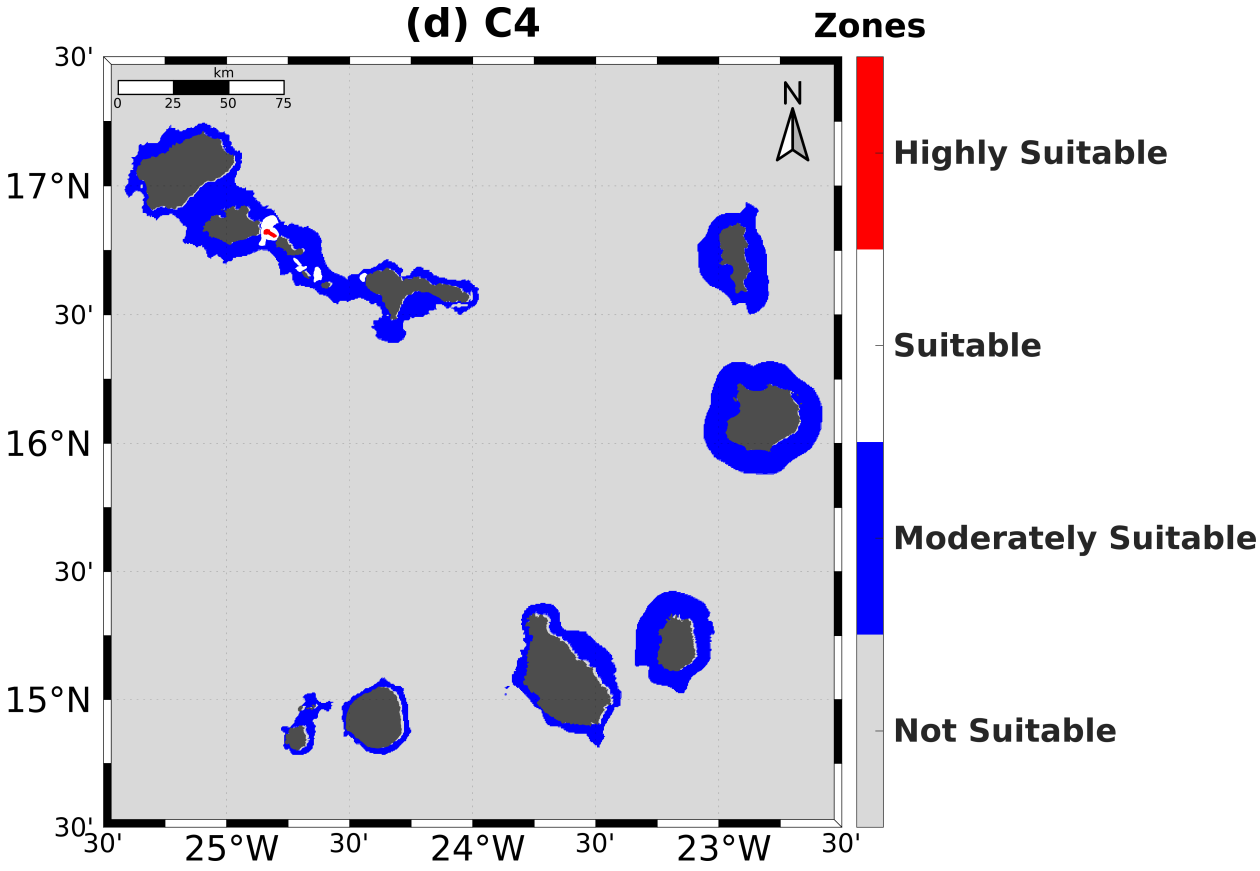

Fig. 7. Optimal OCE zonation for Cabo Verde based on AHP results under three weighting conditions: (a) C1 (equal priority to all criteria), (b) C2 (higher importance to energy potential and depth), (c) C3 (energy potential importance increased by 10%), and (d) C4 (C3 with the influence of TC). The black plus markers on (9b) indicate the final selected locations, labeled 1 to 11, corresponding to station names discussed later in the paper.

3.4. Energy and Site Characterizations at Hotspot Locations

The time series of current speed and current density at the 11 optimal sites, designated as Stations 1 to 11 (St1–St11), exhibit significant site to site variations (Fig. 8a–f). Broadly grouping them into three based on proximity (i.e., Stations 1–4, 5–7, and 8–11), Station 2 exhibits the highest current speed and density among all stations, with speeds frequently exceeding 0.7 m/s, often surpassing 1 m/s, and reaching up to 1.8 m/s (Fig. 8a, d). Station 3 also experiences strong currents, often exceeding 1 m/s, while Station 4 rarely surpasses this threshold. Station 1 records the lowest currents in this subgroup, barely reaching 0.7 m/s. This current variation is reflected in the current density, where Station 2 consistently exhibits the highest values, followed by Station 3. The current

density at Station 2 frequently approaches 2000 W/m² (2.8 MW) and occasionally exceeds 3000 W/m² (4.2 MW). Both current speed and current power density exhibit a clear fortnightly variation, highlighting the role of tidal dynamics.

Among Stations 5 to 7, only Station 5 exhibits current speeds exceeding 1 m/s, while Stations 6 and 7 rarely reach 0.9 m/s (Fig. 8b). Their corresponding current densities are generally below 500 W/m², except for Station 5, which reaches 1000 W/m² (2.1 MW) or more at peak times (Fig. 8e). The current speed and densities at Station 5 surpass Station 1 and 4 from previous subgroup, indicating some localized energy potential. Stations 8 to 11 have the lowest current speeds and densities across the study area, with currents rarely reaching 0.8 m/s (Fig. 10c, f). This results in current densities below 250 W/m² (0.35 MW), occasionally reaching 300 W/m² (0.42 MW).

The mean current speed, OCD, CoV, and MVI for each station are summarized in Table 3. Stations 2, 3, and 5 showed mean speeds above 0.7 m/s, while Stations 4, 6, and 7 remain above 0.5 m/s. The remaining stations register mean speeds below 0.5 m/s. Station 2 stands out with the most stable energy potential, indicated by its low OCD and MVI, making it the most reliable site for energy extraction. Stations 3 and 5 exhibit moderate OCD and MVI values, suggesting some variability but still significant energy potential. In contrast, Stations 4, 6, and 7 display moderate energy potential with greater variability.

The mean current speed, OCD, CoV, and MVI over the entire time period for each station is presented in Table 3. As seen, Stations 2, 3, and 5 have the highest current speed and density throughout the study. The mean current speed for the three stations is above 0.7 m/s. Stations 4, 6, and 7 are above 0.5 m/s while the rest are below 0.5 m/s. OCD for Station1 is above 1000 W/m^2, and as for Stations 3 and 5, OCD is above 240 W/m^2, while OCD for Stations 4, 6 and 7 have values close to 100 W/m^2. Station 2 also has the lowest OCD and MVI indicating stable energy can be extracted, while Stations 3 and 5 have moderate OCD and MVI as compared to the rest. Stations 4, 6, and 7 show some potential for energy variability.

Stations 5, 6, 7, and 11 are situated at depths exceeding 100 m, whereas the remaining stations are shallower, with several below 50 m depth. Notably, Stations 2, 3, and 9 are extremely shallow at 10 m, 10 m, and 18 m, respectively. Except for Station 10 (~7.45 km offshore), all other stations are located within 2–5 km from the shore, making them viable for nearshore energy extraction. Since waves are generally stronger in northern CV (the windward side), with shadow zones located

on the southern side of each island, all selected points exhibit mean significant wave heights between 1.2 and 1.7 m. Stations 2, 4, 5, 7, and 11 show mean values exceeding 1.6 m (Supplementary Fig. S8).

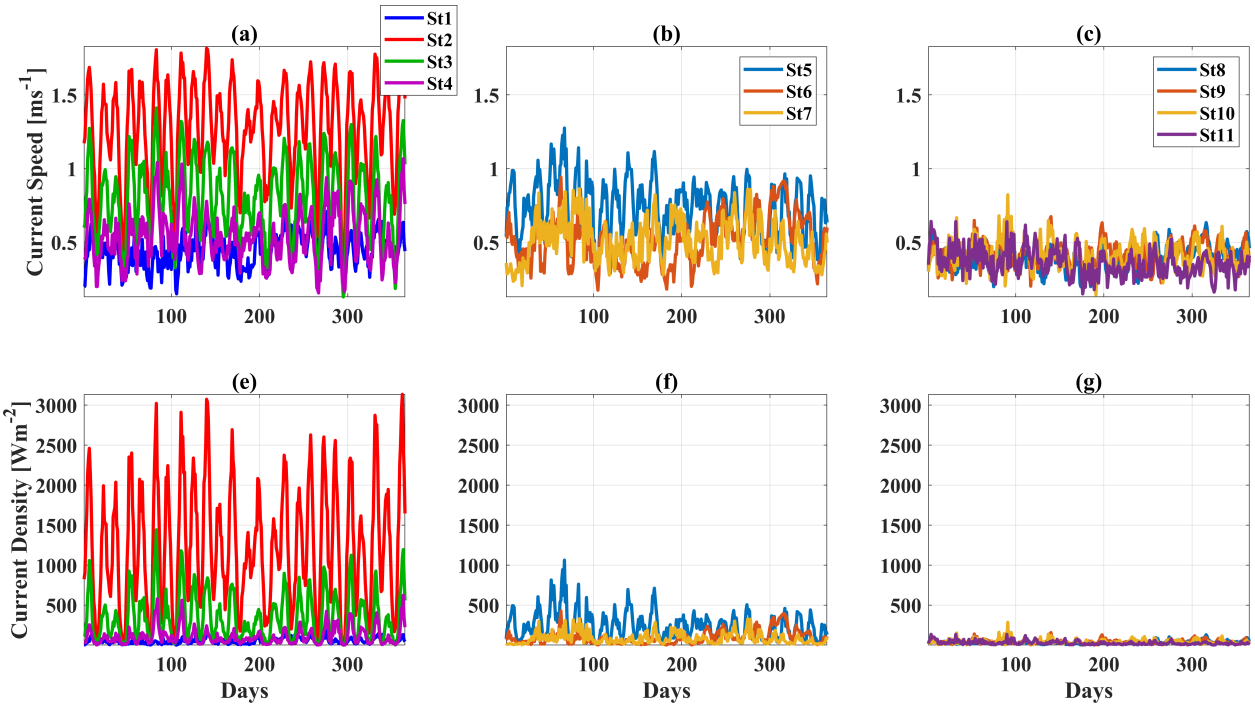

Fig. 8. Daily variations in current speed and densities at selected hotspot sites in the archipelago (see Table 3 for locations).

4. Discussion

The oceanographic dynamics of Cabo Verde are primarily governed by the Intertropical Convergence Zone (ITCZ) and trade winds[31], creating complex seasonal circulation patterns that drive variability in ocean current speed and density. The region is dominated by the westward-flowing North Equatorial Current (NEC), influenced by key oceanographic features such as the CV Frontal Zone and the Guinea Dome, both of which respond to seasonal shifts in the ITCZ[31,50]. Additionally, mesoscale eddies form through wind-topography interactions, and they interact with incoming background eddies propagating from the West African coast and surrounding waters[32]. Tidal forcing can also generate strong currents year-round, particularly in coastal regions and narrow straits between adjacent islands. These processes contribute to pronounced spatial and temporal variability in ocean current speed and density (Figs. 3, 4, 5, 6; Table 3).

As a result, very strong currents (reaching and exceeding 0.9 m/s year-round) occur between the northwest island, specifically between São Vicente and Santa Luzia, and between Santa Luzia and the islet near São Nicolau (Islet 1). These currents are clearly driven by tidal forces, as evidenced by the dominant fortnightly variations, characteristic of the spring-neap tidal cycle (Fig. 8). Furthermore, such strong currents were absent in model simulations from CMEMS and HYCOM that do not incorporate tidal forcing (Supplementary Fig. S3). Relatively strong currents are also found in north São Nicolau and between Bao Vista and Maio, and around the tips of islands like Sal, and Santiago, these are mostly created by mix of tides and mesoscale eddies. These result in high mean current densities exceeding 200 W/m² between São Vicente and uninhabited island of Santa Luzia, Santa Luzia and Islet 1, occurring year-round. Current density values of above 80–100 W/m² are also found in some other locations (Maio and Boa vista, northern Santiago) which vary throughout the year. These values reach around 150 W/m² or more at the 95th percentile for those other locations (Fig. 5). Most areas exhibiting high to moderate current velocities and current densities also correspond with low MVI and CoV values, indicating stable energy availability driven by regular tidal cycles discussed above. These regions present promising potential for current energy development. In contrast, areas with high MVI and CoV, particularly in the southwest of the study region (Fig. 8), are likely influenced by transient eddies, suggesting greater variability and reduced predictability.

The AHP analysis used to identify and characterize optimal locations for OCE reveals that whether equal importance is assigned to all criteria and sub-criteria (C1), or higher priority is given to specific factors such as OCD and depth (C2, C3 and C4), the most suitable sites for OCE are predominantly located in shallow waters within approximately 10 km of the coast. However, the incorporation of TC exposure in C4 further refines the zonation to clearly define the most suitable zones. The eastern and southern islands, including Sal, Boa Vista, Maio, Santiago, Fogo, and Brava have high TC exposure probability with most storms passing through Boa Vista and the center of CV. The final AHP zonation is generally expected to be sensitive to the relative weighting of criteria and sub-criteria, aligning with findings from previous studies[17,18]. Nevertheless, Stations 2, 3, and 5 emerge as the most promising OCE energy hotspot zones. Stations 2 and 3, with depths of approximately 10 m, are suitable for piling structures, while Station 5, at depths exceeding 250 m, would likely require a moored system. Stations 4, 6, and 7 are moderately viable if a mean current speed around 0.5 m/s is considered sufficient for turbine operation which would require

advanced turbine designs. Furthermore, the high current variability may necessitate adaptive turbine designs, potentially increasing installation and operational costs. Additionally, the extreme depths of Stations 6 and 7, exceeding 500 m, further complicates deployment feasibility.

Beyond offshore suitability, the feasibility of energy extraction sites depends on the stability of coastal infrastructure required for grid connection, including cable landfalls and nearshore substations. We observed that the passage of storms can generate waves close to 4.5 or more in CV, even though several locations have mean wave heights below 1.5 m, with most remaining under 2 m. TCs can also induce massive storm surges, in addition to waves that could impact nearshore currents and bottom shear stress. Hence, in regions exposed to storms, surges and strong wave climates, shoreline morphodynamics and coastal erosion can significantly affect infrastructure reliability. Highly dynamic coastlines may increase the risk of cable exposure, burial failure, or damage to coastal facilities. Therefore, integrating detailed and long-term shoreline vulnerability[7,9], sediment transport processes, and long-term erosion–accretion dynamics[8] represents an important extension of the present framework for future site-specific assessments.

The ocean current and OCD in the study area are comparable or higher to those found in Indonesia, another island nation located near the Equator, which is also transitioning from a fossil fuel-dominated energy portfolio to renewable energy[51-52]. This comparison highlights the potential of OCD in CV. Also, flow amplification in the identified hotspots is driven by bathymetric constriction, headland acceleration, and channelized flow between islands, which enhance current speeds through momentum conservation and pressure-gradient forcing. Similar amplification mechanisms have been documented in Indonesia above. This provides a relevant physical benchmark that strengthens the scientific validity and contextual relevance of our findings. Nonetheless, the mean ocean current and OCD values at some of the selected stations as indicated above, along with their ranges and maximums (Fig. 8), suggest that ocean current and OCD may exhibit some temporal variability in the archipelago. Nonetheless, other forms of extractable marine energy, such as wave energy, and their fundamental variables, like wave height, may exhibit temporal variability that aligns with or diverges from that of ocean currents and OCD, depending on the dominant driving processes[27,53,54].

Finally, OCE represents a viable means to convert the ocean's limitless energy into electricity via marine current turbines[12], and its exploitation could revolutionize energy production in CV. This

study shows that OCE is feasible for CV with optimum locations in between the northern islands. Bernardino et al.[29] had earlier shown that there is a huge potential for wave energy in the western and northern part of the islands. Hence, each island could have its own marine renewable or mix of renewables close to the shore based on the available resources. One key advantage for CV is its existing land-based wind energy infrastructure, which allows for partial technology transfer to OCE systems due to similarities in power conversion and grid integration[11]. Considering the seasonal, monthly, and daily variability, it will be essential to integrate the OCE renewable with a centralized storage method such as marine gravity so that both can share the same platform if nearshore system is considered[55,56]. In addition to electricity generation, ocean energy like OCE can support localized applications such as seawater desalination[56] and green hydrogen production[57], utilizing the electricity produced directly at or near the generation site, making it an ideal fit for island nations like CV. The highlighted composite energy system can be a prototype for other coastal sub-Saharan African nations and the rest of the world subject to further multicriteria analyses of the storage systems.

This study has some limitations that provide opportunities for further refinement. For example, the incorporation of higher-resolution bathymetric datasets, including survey-based products or data-driven bathymetry reconstruction approaches[58] could improve the representation of complex underwater terrain. This is especially important for nearshore, inter-island, and islet bathymetry, along with localized slopes, ridges, and substrate heterogeneity. In the present study, ETOPO22 data at 15 arc-second resolution was used as the depth criterion; although the 450 m grid is suitable for regional macro-siting, it is not detailed enough to resolve seabed features required for engineering design and safe turbine support structures. Recent advances in explainable machine learning further suggest that adaptive normalization and spatial feature engineering may help capture such seabed complexity more effectively[58]. In addition, extending the temporal resolution of ocean current data would further strengthen the analysis. While the model performs well against drifter and captures tidal validation, multi-year or climatological simulations would better capture interannual variability associated with climate modes. Finally, although AHP provides a transparent and widely adopted framework for structuring complex decisions[59], it remains subject to limitations inherent in judgment-based MCDA methods. While the multi-scenario sensitivity analysis implemented in this study provides a robust assessment of weighting uncertainty,

advanced approaches such as fuzzy AHP, Bayesian MCDA, and Monte Carlo weighting are valuable extensions to quantify for uncertainty.

5. Summary and Conclusion

This study develops a transferable, risk-informed MCDA framework that integrates high-resolution hydrodynamics, environmental constraints, and extreme-event exposure for ocean current energy planning in Small Island Developing States. It also introduces a methodology for integrating TC risk into the MCDA model. The high-resolution ocean model resolves detailed current structures around the archipelago, including strong currents flowing between the islands. The multicriteria approach, combined with sensitivity analysis, identifies optimal energy hotspots based on key criteria and sub-criteria including energy potential (current speed, power density, and variability), environmental constraints (PAs), techno-economic factors (D2C, depth, and TC exposure), and wave climate.

Our finding reveals that OCE resources in CV show significant spatial variability and short-term fluctuations, shaped by large-scale currents, mesoscale eddies, and particularly tidal forcing. These tidal influences often generate strong and reliable currents near coastlines and in narrow straits or channels. The highest current speed and power density are between the northern islands of CV, with moderately high values in northern São Nicolau, Sal, and Santiago, as well as between Boa Vista and Maio. However, only a few locations meet the key criteria for viable OCE extraction, considering depth, proximity to shore, current intensity, and stability. The most promising sites are between São Vicente and Santa Luzia, as well as between Santa Luzia and Islet 1 (Stations 2, 3, and 5). These areas are also free from major shipping routes and protected areas, minimizing conflicts with other maritime activities. Importantly, they are situated in zones with lower exposure risk to tropical cyclones and weaker wave conditions, enhancing their reliability and long-term sustainability. It is important that in situ measurements be conducted in these locations to validate the findings suggested by our model simulations, as the lack of observational data represents a limitation.

Cabo Verde has the potential to harness OCE, particularly in these optimal locations, complementing other marine renewable energy sources such as wave energy in the northern region. Given the country's existing wind energy infrastructure, certain technologies can be adapted for OCE systems, facilitating integration into the energy mix. Additionally, energy storage solutions

could enhance the reliability and sustainability of marine energy for the archipelago, contributing to a more stable and resilient renewable energy system.

Table 3. Mean and variability of ocean current (m/s) and OCD (Wm^{-2}) for Cabo Verde

	Lon	Lat	depth	D2C	mean current speed (m/s)	mean OCD (Wm-2)	CoV (OCD)	MVI OCD
St1	-25.1	16.9	-69	3.26	0.44	53.2	0.15	0.19
St2	-24.8	16.8	-10	3.74	1.27	1252.3	0.13	0.07
St3	-24.7	16.7	-10	3.73	0.81	353.3	0.18	0.12
St4	-24.6	16.6	-51	1.28	0.54	107.6	0.22	0.19
St5	-24.4	16.7	-272	2.49	0.74	244.2	0.16	0.16
St6	-24.3	16.5	-558	2.07	0.52	96.5	0.20	0.39
St7	-24.0	16.6	-815	2.92	0.51	82.5	0.18	0.30
St8	-23.0	16.7	-34	2.77	0.40	36.3	0.13	0.22
St9	-22.9	16.0	-18	2.42	0.42	42.7	0.14	0.15
St10	-23.1	15.4	-34	7.45	0.41	42.1	0.16	0.12
St11	-23.7	15.3	-217	3.46	0.36	28.9	0.18	0.21

Acknowledgements

The authors would like to acknowledge West African Science Service Center on Climate Change and Adapted Land-Use (WASCAL), and the Federal Ministry of Education and Research, Germany, for sponsoring this research.

Funding

Not applicable.

Data availability

The data and code used in this study are publicly available at Zenodo (https://zenodo.org/uploads/15485734). All other data sources are described in the manuscript.

References

1. Bouckaert, S. *et al. Net zero by 2050: A roadmap for the global energy sector.* International Energy Agency (2021).
2. Masson-Delmotte, V. *et al. Climate Change 2021: The Physical Science Basis. Contribution of Working Group I to the Sixth Assessment Report of the Intergovernmental Panel on Climate Change.* Cambridge University Press, Cambridge, United Kingdom and New York, NY, USA (2021). doi:10.1017/9781009157896.
3. Renewable energy statistics 2025. **https://www.irena.org/Publications/2025/Jul/Renewable-energy-statistics-2025** (2025).
4. James, S., Christopher, W. & Lauren, R. A global cross-resource assessment of offshore renewable energy. *Renewable and Sustainable Energy Reviews* **215**, 115563 (2025).
5. Pennock, S., Noble, D. R., Vardanyan, Y., Delahaye, T. & Jeffrey, H. A modelling framework to quantify the power system benefits from ocean energy deployments. *Applied Energy* **347**, 121413 (2023).
6. Sadoughipour, M., VanZwieten, J. & Tang, Y. Drifter-based global ocean current energy resource assessment. *Renewable Energy* **244**, 122576 (2025).
7. Durap, A. Multi-decadal spatiotemporal shoreline vulnerability assessment (1987–2025): integrating erosion-accretion dynamics for disaster risk reduction across 90 coastal transects. *Nat Hazards* **121**, 22981–23019 (2025).
8. Durap, A. Beachface steepness modulates erosion but not recovery: Multi-decadal spatiotemporal shoreline evidence across 390 transects. *Journal of Sea Research* **208**, 102644 (2025).
9. Brempong, E. K. et al. Understanding the drivers of Extreme Coastal Water Levels in West Africa from oceanic and climatic processes. *Discov Oceans* **3**, 23 (2026).
10. Nordman, E., Barrenger, A., Crawford, J., McLaughlin, J. & Wilcox, C. Options for Achieving Cape Verde's 100% Renewable Electricity Goal: A Review. *Island Studies Journal* **14**, (2019).
11. Chen, H. *et al.* Attraction, Challenge and Current Status of Marine Current Energy. *IEEE Access* **6**, 12665–12685 (2018).
12. Gu, Y. *et al.* Status and Challenges of Marine Current Turbines: A Global Review. *Journal of Marine Science and Engineering* **12**, (2024).
13. Ghosh, S., Chakraborty, T., Saha, S., Majumder, M. & Pal, M. Development of the location suitability index for wave energy production by ANN and MCDM techniques. *Renewable and Sustainable Energy Reviews* **59**, 1017–1028 (2016).
14. Salvador, C. B., Arzaghi, E., Yazdi, M., Jahromi, H. A. F. & Abbassi, R. A multi-criteria decision-making framework for site selection of offshore wind farms in Australia. *Ocean & Coastal Management* **224**, 106196 (2022).
15. Majidi, A. G. *et al.* Development of a multi-criteria decision-making tool for combined offshore wind and wave energy site selection. *Applied Energy* **384**, 125422 (2025).
16. Shao, M. *et al.* A review of multi-criteria decision making applications for renewable energy site selection. *Renewable Energy* **157**, 377–403 (2020).

17. Johnston, B., Al Kez, D., McLoone, S. & Foley, A. Offshore wind potential in Northern Ireland using GIS multi-criteria assessment. *Applied Energy* **378**, 124764 (2025).
18. Solbrekke, I. M. & Sorteberg, A. Norwegian offshore wind power—spatial planning using multi-criteria decision analysis. *Wind Energy* **27**, 5–32 (2024).
19. Kirby, K., Rennie, C. D., Cousineau, J., Ferguson, S. & Nistor, I. Impacts of seasonal flow variation on riverine hydrokinetic energy resources and optimal turbine location – Case study on the Rivière Rouge, Québec, Canada. *Renewable Energy* **210**, 364–374 (2023).
20. Bao, M. *et al.* Site selection for offshore renewable energy platforms: A multi-criteria decision-making approach. *Renewable Energy* **229**, 120768 (2024).
21. Dallavalle, E., Zanuttigh, B., Contestabile, P., Giuggioli, A. & Speranza, D. Improved methodology for the optimal mixing of renewable energy sources and application to a multi-use offshore platform. *Renewable Energy* **210**, 575–590 (2023).
22. Ticona Rollano, F., García Medina, G., Yang, Z. & Copping, A. Resource assessment of ocean thermal energy conversion in Puerto Rico and U.S. Virgin Islands. *Renewable Energy* **246**, 122907 (2025).
23. UNEP. Atlas of Africa Energy Resources. United Nations Environment Programme, Nairobi (2017).
24. Qing, X. Statistical analysis of wind energy characteristics in Santiago island, Cape Verde. *Renewable Energy* **115**, 448–461 (2018).
25. Pombo, D. V., Martinez-Rico, J. & Marczinkowski, H. M. Towards 100% renewable islands in 2040 via generation expansion planning: The case of São Vicente, Cape Verde. *Applied Energy* **315**, 118869 (2022).
26. Pombo, D. V., Martinez-Rico, J., Spataru, S. V., Bindner, H. W. & Sørensen, P. E. Decarbonizing energy islands with flexibility-enabling planning: The case of Santiago, Cape Verde. *Renewable and Sustainable Energy Reviews* **176**, 113151 (2023).
27. Monteiro, W. M. L., Sarmento, A. J., Fernandes, A. J. & Fernandes, J. M. Statistical Analysis of Wave Energy Resources Available for Conversion at Natural Caves of Cape-Verde Islands. *Ocean Science Discussions* 1–23 (2016) doi:10.5194/os-2015-108.
28. Leger Monteiro, W. M. & Sarmento, A. Analysing the Possibility of Extracting Energy from Ocean Waves in Cabo-Verde to Produce Clean Electricity - Case-Study: the Leeward Islands. *Int. J. Renew. Energy Dev.* **8**, 103–112 (2019).
29. Bernardino, M., Rusu, L. & Guedes Soares, C. Evaluation of the wave energy resources in the Cape Verde Islands. *Renewable Energy* **101**, 316–326 (2017).
30. Fernandes, M. J., Lázaro, C., Santos, A. M. P. & Oliveira, P. Oceanographic characterization of the Cape Verde region using multisensor data. In Proceedings of the 2004 Envisat & ERS Symposium (ESA SP-572), 6–10 September 2004, Salzburg, Austria. Eds. Lacoste, H. & Ouwehand, L. European Space Agency (2005)**.**
31. Pelegrí, J. L., Peña-Izquierdo, J., Machín, F., Meiners, C. & Presas-Navarro, C. Oceanography of the Cape Verde Basin and Mauritanian Slope Waters. in *Deep-Sea Ecosystems Off Mauritania: Research of Marine Biodiversity and Habitats in the Northwest African Margin* (eds. Ramos, A., Ramil, F. & Sanz, J. L.) 119–153 (Springer Netherlands, Dordrecht, 2017). doi:10.1007/978-94-024-1023-5_3.

32. Cardoso, C., Caldeira, R. M. A., Relvas, P. & Stegner, A. Islands as eddy transformation and generation hotspots: Cabo Verde case study. *Progress in Oceanography* **184**, 102271 (2020).
33. Lin, S., Sheng, J., Zheng, J. & Tao, A. Convergence and divergence of storm waves induced by multi-scale currents: Observations and coupled wave-current modeling. *Coastal Engineering* **194**, 104627 (2024).
34. Göteman, M. *et al.* Resilience of offshore renewable energy systems to extreme metocean conditions: A review. *Renewable and Sustainable Energy Reviews* **216**, 115649 (2025).
35. Hallowell, S. T. *et al.* Hurricane risk assessment of offshore wind turbines. *Renewable Energy* **125**, 234–249 (2018).
36. Gula, J., Theetten, S., Cambon, G. & Roullet, G. *Description of the GIGATL simulations*. Zenodo, version 1.1 (2021). doi:10.5281/zenodo.4948523.
37. Shchepetkin, A. F. & McWilliams, J. C. The regional oceanic modeling system (ROMS): a split-explicit, free-surface, topography-following-coordinate oceanic model. *Ocean Modelling* **9**, 347–404 (2005).
38. Auclair, F. *et al.* Coastal and Regional Ocean COmmunity Model (v2.1.0). Zenodo (2025). doi: 10.5281/zenodo.15064113.
39. Oladejo, H. O. *et al.* Wind forcing, source term and grid optimization for hurricane wave modelling in the Gulf of Mexico. *Coastal Engineering* **197**, 104692 (2025).
40. Boretti, A. & Castelletto, S. Advancements and challenges in tidal stream and oceanic current turbines: an overview of current technologies and future prospects. *Mar Dev* **3**, 10 (2025).
41. Rizal, A. M. & Ningsih, N. S. Ocean wave energy potential along the west coast of the Sumatra island, Indonesia. *J. Ocean Eng. Mar. Energy* **6**, 137–154 (2020).
42. ETOPO Global Relief Model. *National Centers for Environmental Information (NCEI)* https://www.ncei.noaa.gov/products/etopo-global-relief-model (2022).
43. MacFerrin, M., Amante, C., Carignan, K., Love, M. & Lim, E. The Earth Topography 2022 (ETOPO 2022) global DEM dataset. *Earth System Science Data* **17**, 1835–1849 (2025).
44. Knapp, K. R., Kruk, M. C., Levinson, D. H., Diamond, H. J. & Neumann, C. J. The International Best Track Archive for Climate Stewardship (IBTrACS). https://doi.org/10.1175/2009BAMS2755.1 (2010) doi:10.1175/2009BAMS2755.1.
45. Soh, Y., Hae, Y., Mehmood, A., Ashraf, R. H. & Kim, I. Performance Evaluation of Various Functions for Kernel Density Estimation. (2013).
46. Węglarczyk, S. Kernel density estimation and its application. *ITM Web Conf.* **23**, 00037 (2018).
47. Oladejo, H. O. et al. Development of a hybrid modeling framework for optimizing wind forcing and enhancing hurricane wave simulation. Preprint at http://dx.doi.org/10.2139/ssrn.6575414 (2026).
48. Saaty, T. L. Decision making with the analytic hierarchy process. *International Journal of Services Sciences* **1**, 83–98 (2008).
49. Esteban, M. & Leary, D. Current developments and future prospects of offshore wind and ocean energy. *Applied Energy* **90**, 128–136 (2012).

50. Peña-Izquierdo, J. *et al.* The continental slope current system between Cape Verde and the Canary Islands. *Sci. mar.* **76**, 65–78 (2012).
51. Purba, N. P. et al. Preliminary Research of Using Ocean Currents and Wind Energy to Support Lighthouse in Small Island, Indonesia. *Energy Procedia* 47, 204–210 (2014).
52. Purba, N. P., Pranowo, W. S., Ndah, A. B. & Nanlohy, P. Seasonal variability of temperature, salinity, and surface currents at 0° latitude section of Indonesia seas. *Regional Studies in Marine Science* 44, 101772 (2021).
53. Rizal, A. M. & Ningsih, N. S. Description and variation of ocean wave energy in Indonesian seas and adjacent waters. *Ocean Engineering* **251**, 111086 (2022).
54. Adesina, R. B., He, Z., Oladejo, H. O., Dada, O. A. & Ajibade, H. J. High-resolution wave modeling of the Southwestern Nigerian coastal shelf: Implications on geomorphic contrasts between barrier-lagoon and mud coasts. *Marine Geology* **470**, 107253 (2024).
55. Wang, Z., Carriveau, R., Ting, D. S.-K., Xiong, W. & Wang, Z. A review of marine renewable energy storage. International Journal of Energy Research 43, 6108–6150 (2019).
56. Hunt, J. D. *et al.* Buoyancy Energy Storage Technology: An energy storage solution for islands, coastal regions, offshore wind power and hydrogen compression. *Journal of Energy Storage* **40**, 102746 (2021).
57. Taroual, K. *et al.* Hybrid marine energy and AI-driven optimization for hydrogen production in coastal regions. *International Journal of Hydrogen Energy* **118**, 80–92 (2025).
58. Durap, A. Explainable machine learning for bathymetric mapping: adaptive normalization and feature engineering in complex seabed terrains. *Ocean Sci*. J. 60, 52 (2025).
59. Munier, N. & Hontoria, E. Uses and Limitations of the AHP Method: A Non-Mathematical and Rational Analysis. (*Springer International Publishing*, Cham, 2021). doi:10.1007/978-3-030-60392-2.